Article

Membrane Protein Structures in Native Cellular Membranes Revealed by Solid-State NMR Spectroscopy

Yan Zhang,[||] Yuefang Gan,[||] Weijing Zhao,[||] Xuning Zhang, Yongxiang Zhao, Huayong Xie,* and Jun Yang*

Cite This: JACS Au 2023, 3, 3412−3423

Read Online

ACCESS | Metrics & More | Article Recommendations | Supporting Information

ABSTRACT: The structural characterization of membrane proteins within the cellular membrane environment is critical for understanding the molecular mechanism in their native functional context. However, conducting residue site-specific structural analysis of membrane proteins in native membranes by solid-state NMR faces challenges due to poor spectral sensitivity and serious interference from background protein signals. In this study, we present a new protocol that combines various strategies for cellular membrane sample preparations, enabling us to reveal the secondary structure of the mechanosensitive channel of large conductance from *Methanosarcina acetivorans* (*Ma*MscL) in *Escherichia coli* inner membranes. Our findings demonstrate the feasibility of achieving complete resonance assignments and the potential for determining the 3D structures of membrane proteins within cellular membranes. We find that the use of the BL21(DE3) strain in this protocol is crucial for effectively suppressing background protein labeling without compromising the sensitivity of the target protein. Furthermore, our data reveal that the structures of different proteins exhibit varying degrees of sensitivity to the membrane environment. These results underscore the significance of studying membrane proteins within their native cellular membranes when performing structural characterizations. Overall, this study opens up a new avenue for achieving the atomic-resolution structural characterization of membrane proteins within their native cellular membranes, providing valuable insights into the nativeness of membrane proteins.

KEYWORDS: solid-state NMR, membrane protein, native cellular membrane, structure, nativeness
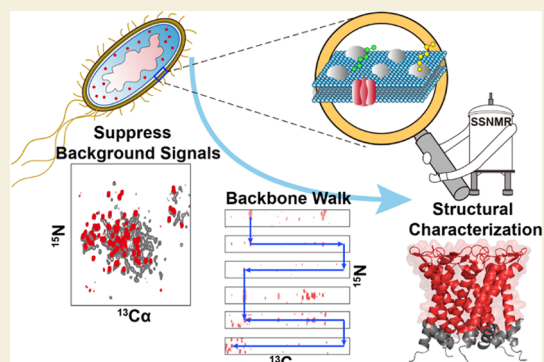
Membrane proteins (MPs) function within a highly intricate and diverse membrane environment, where the presence of various membrane components and complex physical and chemical properties of the membrane significantly influence their functions and structures.[1] Currently, the majority of MP structures in the Protein Data Bank (PDB) have been determined in simplified membrane mimic environments, such as detergent micelles, lipidic cubic phases, nanodiscs, and synthetic lipid bilayers.[2] This is primarily due to the exceptional complexity of the cellular membranes. However, these simplified membrane mimics, particularly detergents, are likely to disrupt the structures of MPs, leading to a misinterpretation of their structural mechanisms.[3] Therefore, accurately elucidating the folding, structure, and dynamics of MPs within their native cellular membrane environments is crucial to understanding their functions in physiological membranes.

Various techniques, including cellular solid-state NMR,[4−7] in-cell NMR,[8] electron paramagnetic resonance (EPR),[9] fluorescence,[10] and cellular cryo-electron tomography (cryo-ET),[11] enable the study of proteins within cellular environments. Among these techniques, cellular solid-state NMR has

shown promising potential for directly analyzing the structures of MPs in native cellular membranes.[6] In contrast to *in vitro* solid-state NMR studies that rely on artificially prepared proteoliposomes, cellular solid-state NMR allows for the investigation of MPs without the need for purification and reconstitution procedures during sample preparation, thus eliminating the use of detergents. Significant progress has been made in sample preparations and detection techniques, including protein enrichment,[12−14] suppression of background proteins,[15−17] and the use of dynamic nuclear polarization (DNP) to enhance NMR sensitivity.[18−20] Using solid-state NMR, the structures of several MPs within cellular membranes have been characterized, including Anabaena sensory rhodopsin (ASR),[17] the K⁺ channel KcsA,[21] YidC,[22] the LR11 (SorLA) transmembrane domain,[23] the M2 proton channel,[24]
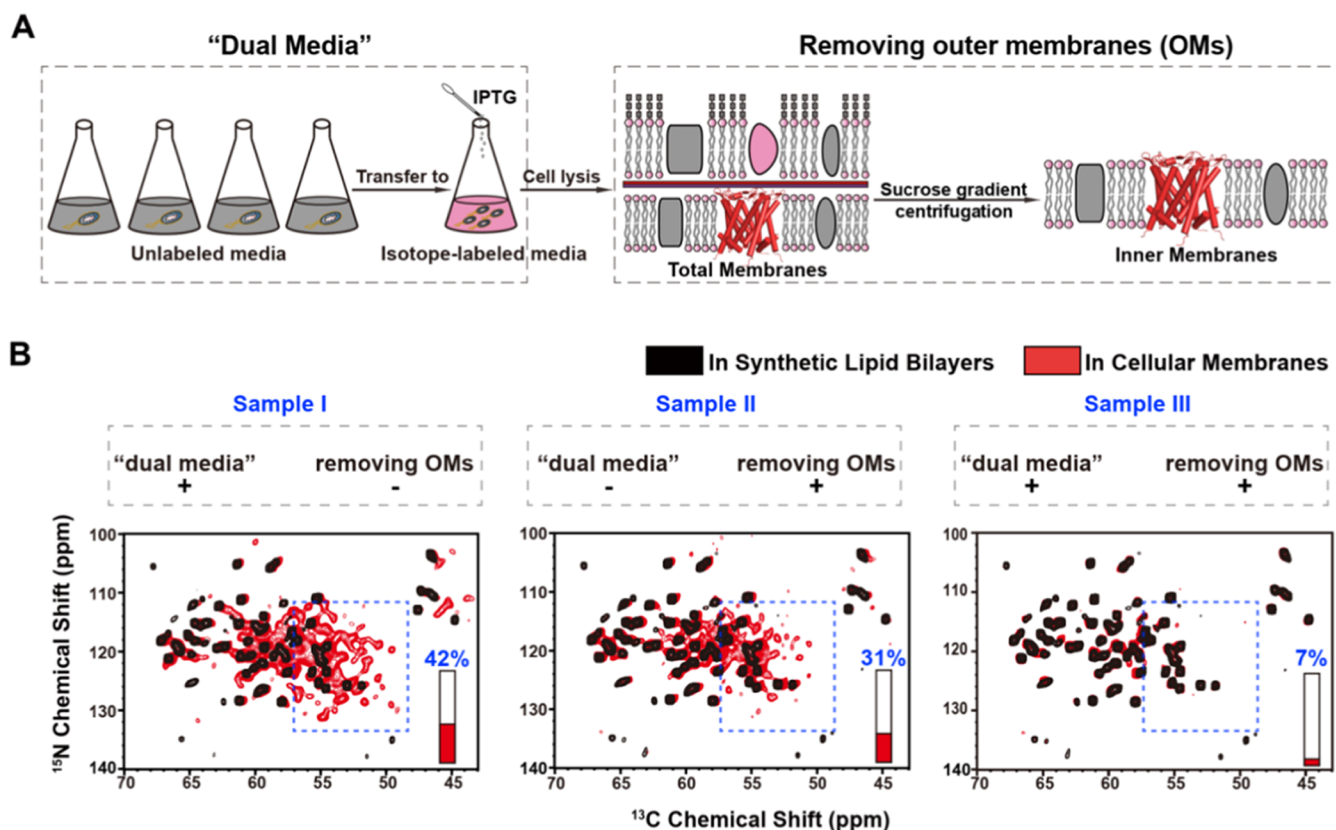
Figure 1. High-sensitivity and high-resolution solid-state NMR spectra of *Ma*MscL in native cellular membranes with minimum interference of background protein signals by combining various techniques in preparing a cellular membrane sample. (A) Preparation procedure for native cellular membrane samples of *Ma*MscL, with further details available in the Experimental Section. (B) Superimposition of 2D NCA spectra of *Ma*MscL in native cellular membranes prepared using "dual media" but without removing OMs (sample I), with removing OMs but without using "dual media" (sample II), and with using "dual media" and removing OMs (sample III). All samples are prepared using the BL21(DE3) strain. The spectral regions containing typical signals from background proteins are highlighted by blue boxes. Isotope-labeled background proteins accounted for 42, 31, and 7% of all inner membrane components in samples I, II, and III, respectively, which are indicated by red rectangles.

Mistic,[25] the *β*-barrel assembly machinery (BAM) complex,[26] and Yersinia adhesin A (YadA).[27]

However, cellular solid-state NMR encounters several technical limitations, including (i) limited abundance of the protein of interest, resulting in poor spectral sensitivity, and (ii) high spectral overlap caused by abundant labeled background proteins. These challenges have greatly hindered the widespread application of cellular solid-state NMR.[5,6,28] To date, residue site-specific structural characterization of membrane proteins in native membranes has not yet been achieved due to the lack of complete resonance assignments. Such assignments necessitate sufficient spectral sensitivity while minimizing interference from the background protein signals.

In this study, we demonstrate the feasibility of achieving residue site-specific structural analysis of MPs in cellular membranes using solid-state NMR. We present a new protocol for cellular membrane preparations that allows for the nearly complete suppression of background protein signals while maintaining high spectral sensitivity for the target protein. Our protocol combines various strategies to enhance the concentration of the target protein and suppress the labeling of background proteins. These strategies include optimizing expression conditions and strains, utilizing "dual media", and removing nontarget membrane components. Importantly, we found that the use of the BL21(DE3) strain in this protocol plays a crucial role in completely suppressing the labeling of

background proteins. Our results provide evidence of the potential of this protocol for collecting distance restraints to facilitate structure determination of MPs by cellular solid-state NMR.

RESULTS

High-Quality Solid-State NMR Spectra of *Ma*MscL in *Escherichia coli* Inner Membranes by Combining Various Strategies in Sample Preparations

We first analyzed the structure of a membrane protein, the mechanosensitive channel of large conductance from *Methanosarcina acetivorans* (*Ma*MscL), in *E. coli* cellular membranes. *Ma*MscL functions as a homopentamer, with each subunit comprising two transmembrane helices.[29] Previously, we had achieved nearly complete resonance assignments of *Ma*MscL in synthetic lipid bilayers by solid-state NMR.[30] In this study, we obtained high-quality solid-state NMR spectra of *Ma*MscL in *E. coli* cellular membranes by combining various strategies. First, we optimized various expression conditions, such as temperature, additives, pH, and induction time, to enhance the yield of *Ma*MscL per liter of culture (up to ~40 mg/L). The subsequent steps for preparing cellular membrane samples are shown in Figure 1A. Specifically, *E. coli* cells were grown in unlabeled media (LB) until the exponential phase, followed by resuspension in isotopically labeled M9 media and induced with IPTG. After cell lysis, the total cell membranes
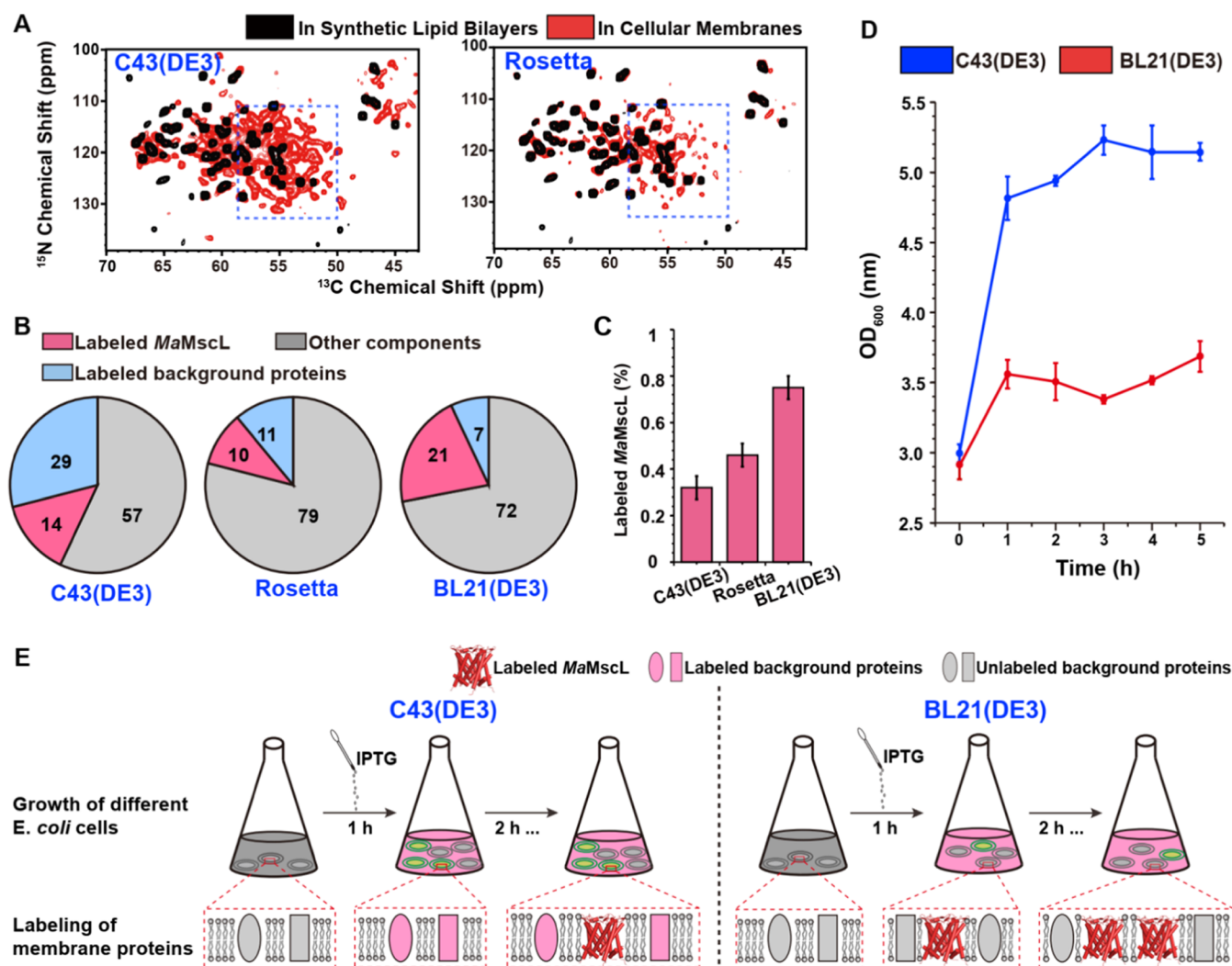
Figure 2. Labeling of background protein was suppressed in the cells using the BL21(DE3) strain by reducing the growth of new cells during the induction time. (A) Superimposition of 2D NCA spectra of *Ma*MscL in native cellular membranes prepared using different expression strains and reconstituted in synthetic lipid bilayers. The spectral regions containing typical signals from background proteins are highlighted by blue boxes. The NCA spectra of the native cell membrane sample prepared using the BL21(DE3) strain showed the complete suppression of the background protein signals. (B) Quantitative characterization of different components in native cellular membrane samples prepared using different *E. coli* expression strains. (C) Percentages of labeled *Ma*MscL among the labeled proteins in native cellular membrane samples were prepared using different *E. coli* expression strains. (D) Cell growth monitored by OD600 using *E. coli* expression strains C43(DE3) and BL21(DE3) in isotope-labeled media after the addition of IPTG. (E) Schematic diagram of cell growth and protein labeling during the preparation of native cellular membrane samples using C43(DE3) and BL21(DE3) strains.

were collected, and the outer membrane components were removed through sucrose gradient centrifugation. The resulting inner membrane fragments, comprising labeled *Ma*MscL, labeled and unlabeled background proteins, lipids, and other coexpressed molecular components, were directly utilized for solid-state NMR experiments without purification and reconstitution.

To monitor labeled background proteins in cellular membrane samples prepared by using different approaches, we compared the 2D NCA spectra of *Ma*MscL in cellular membranes with those in synthetic lipid bilayers. The purified *Ma*MscL was reconstituted into synthetic bilayers without containing any background proteins, making its spectrum a reference to identify the background protein signals in cellular membrane spectra. As shown in Figure 1B, the spectra of cellular membrane samples prepared without using "dual media" (sample I) or the removal of outer membranes (OMs)

(sample II) exhibit numerous background protein signals. In contrast, background protein signals can be suppressed in the spectra of cellular membrane samples prepared using a combination of "dual media" and removing outer membrane components (sample III).

We further analyzed the contents of labeled *Ma*MscL and labeled background proteins in these inner membrane samples. The details of the analysis are described in the Experimental Section. As shown in Figures 1B and S1A, labeled *Ma*MscL constituted only approximately 8 and 7% of all inner membrane components in samples I and II, respectively. However, a higher content of labeled *Ma*MscL (21%) was observed in sample III. As a result, the sensitivity of *Ma*MscL in the spectra of sample III was approximately three times that of samples I and II. Additionally, due to the low content of labeled background proteins and the high content of labeled *Ma*MscL in sample III, labeled *Ma*MscL accounted for

approximately 75% of the labeled proteins (Figure S1B). Although the remaining 25% of labeled proteins were background proteins, their signals were not present in the 2D NCA spectra due to their dispersion among various types of background proteins in cellular membranes.

Use of *E. coli* BL21(DE3) Strain Is Critical for the Suppression of Background Protein Labeling

Interestingly, we found that the amount of labeled background proteins in inner membranes varied, depending on the strains used for protein expression. As shown in Figure 2A, strong background protein signals were detected in the NCA spectra of *Ma*MscL in inner membranes expressed using the C43(DE3) and Rosetta strains, while no background protein signals were present in the spectra of the sample prepared using the BL21(DE3) strain. Furthermore, SDS-PAGE analysis in Figure S2 suggested that the removal of OM components can effectively reduce the content of background proteins in cellular membrane samples prepared by using different *E. coli* strains.

To quantify these signal differences, we analyzed the content of labeled *Ma*MscL and background proteins in inner membrane samples prepared by using different *E. coli* strains. As shown in Figure 2B, the content of labeled background protein of all inner membrane components in inner membrane samples using the BL21(DE3) strain (7%) was lower than that using C43(DE3) (29%) and Rosetta (11%) strains. Furthermore, the content of labeled *Ma*MscL was higher in the sample using the BL21(DE3) strain (21%) compared to the samples using the C43(DE3) (14%) and Rosetta (10%) strains. Due to the high content of labeled background proteins and the low content of labeled *Ma*MscL in the samples prepared using C43(DE3) and Rosetta strains, the percentages of labeled *Ma*MscL among the labeled proteins in these two samples are lower (33 and 48%) than that in the sample using the BL21(DE3) strain (75%) (Figure 2C).

What causes these strains to behave differently in expressing and labeling background proteins? To answer this question, we compared the growth of *E. coli* cells in isotope-labeled media after induction by IPTG using BL21(DE3) and C43(DE3) strains. As shown in Figure 2D, the optical density at 600 nm (OD600), a simple method for measuring cell density in the culture, showed only a slight increase from 3.0 to 3.5 during the induction period when using the BL21(DE3) strain. In contrast, the OD600 increased up to 5.0 when utilizing the C43(DE3) strains. We further monitored the expression of labeled *Ma*MscL and background proteins in intermediate states of cell growth by 2D NCA spectra (Figure S3). The relative content of labeled background proteins decreased as the induction time increased (2 h after IPTG induction) in both BL21(DE3) and C43(DE3) strains. Remarkably, more labeled *Ma*MscL and fewer labeled background proteins were observed in the inner membranes of the BL21(DE3) strain. The results from OD600 values and NCA spectra allowed us to interpret why the labeling of background proteins is significantly suppressed in the cellular membrane sample using the BL21(DE3) strain. As shown in Figure 2E, after adding IPTG, C43(DE3) cells utilized the isotopically labeled resource in the media for cell growth, resulting in newly grown cells that contained abundant labeled background proteins. In contrast, BL21(DE3) cells showed little growth in isotope-labeled media during the induction time, and most of the target proteins were expressed in the existing cells, where

the background proteins were unlabeled. The variation in protein expression between C43(DE3) and BL21(DE3) strains can be attributed to differing tolerances for toxicity resulting from MP overexpression.[31]

Additionally, we also measured the growth of *E. coli* cells in isotope-labeled media after induction by IPTG using the Rosetta strain and compared it with the growth of the BL21(DE3) cells. As shown in Figure S4, the OD600 increased from 2.8 to 3.9 after 1 h of IPTG induction when utilizing the Rosetta strain. In contrast, the OD600 of the BL21(DE3) cells only increased from 2.9 to 3.5 during the 1 h induction period. This slight increase in the OD600 of the Rosetta system resulted in a greater number of newly grown cells in isotope-labeled media, which contained labeled background proteins. Moreover, we found a slightly lower expression yield of *Ma*MscL when using the Rosetta strain (~35 mg/L) compared to the BL21(DE3) strain (~40 mg/L), which consequently led to a reduction in the content of *Ma*MscL in cellular membranes. Therefore, the presence of extra rare tRNA codons in the Rosetta strain leads to a decrease in the expression level of *Ma*MscL while simultaneously promoting the labeling of background proteins. As a result, the proportion of labeled *Ma*MscL among the labeled proteins using the Rosetta strain is lower than that using the BL21(DE3) strain.

It is worth noting that several studies have demonstrated the suppression of protein expression in cellular membranes by the antibiotic rifampicin.[5,15] In our previous work, we demonstrated the suppression of background signals in an Aquaporin Z (AqpZ) cellular membrane sample using rifampicin. However, this treatment also resulted in the suppression of nearly half of the AqpZ expression. In this study, we observed that rifampicin effectively suppresses the expression of background proteins in cellular membrane samples of sugar transporter *Vibrio sp.* SemiSWEET (*Vs*SemiSWEET),[32] *Bradyrhizobium japonicum* SemiSWEET (*Bj*SemiSWEET),[33] and *Ma*MscL using the *E. coli* expression strain C43(DE3), as shown in Figures S5A and S6. However, as shown in Figures S5B and S7, rifampicin treatment also suppressed the expression of the target protein (Figure S5C), resulting in a 68% decrease in the signal intensity of *Ma*MscL, which is only 51% of the intensity observed in the sample prepared using the BL21(DE3) strain without rifampicin treatment. The sensitivity of the rifampicin-treated sample is insufficient for acquiring general 3D spectra for resonance assignments. Furthermore, as shown in Figures S5A and S6, background signals were still observed in these spectra, hindering the acquisition of distance constraints for structure determination in 2D $^{13}C-^{13}C$ correlation spectra. In contrast, the use of the BL21(DE3) strain can completely suppress the labeling of background proteins without sacrificing the sensitivity of the target protein.

Secondary Structures of *Ma*MscL in Native Cellular Membranes by *De Novo* Resonance Assignments

Resonance assignment is a critical first step in the residue site-specific structural and dynamic characterization of proteins. In this study, we were able to perform multidimensional solid-state NMR experiments for the resonance assignments of *Ma*MscL, benefiting from its high sensitivity and minimal interference from background proteins in the cellular membrane sample (Figure S8). We have provided a comprehensive list of all solid-state NMR experiments conducted in this study, including those used for resonance
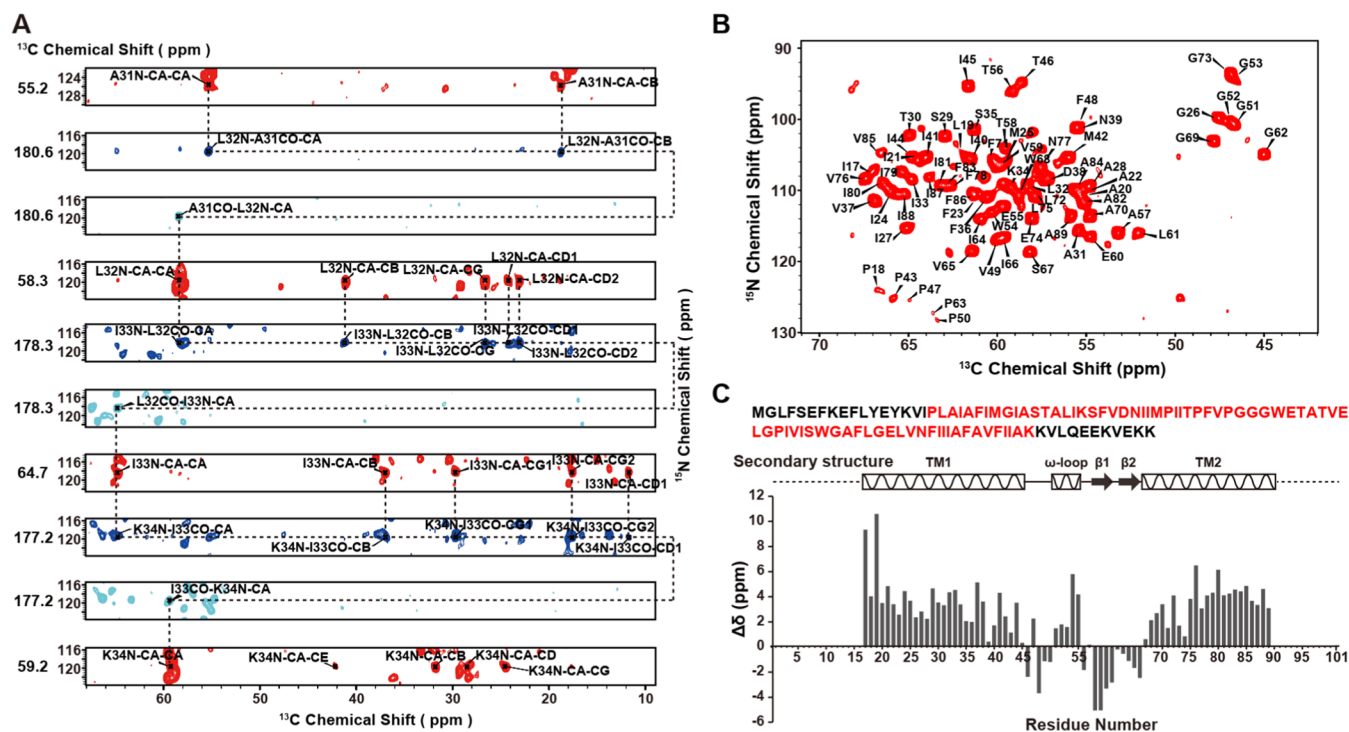
Figure 3. Resonance assignments of *Ma*MscL in native cellular membranes by 3D experiments. (A) Representative sequential assignments of residues A31−K34 of *Ma*MscL in native cellular membranes by 3D NCACX, NCOCX, and CONCA spectra, with dashed lines guiding the backbone walk. (B) 2D NCA spectrum of *Ma*MscL in native cellular membranes with labeling of the assigned signals. (C) Secondary chemical shifts plotted as a function of the residue number, where residues with positive and negative values tend to have α-helical and β-strand structures, respectively. The predicted secondary structures of *Ma*MscL in native cellular membranes are depicted at the top of the figure with zigzag lines denoting α-helical segments, solid lines representing unstructured residues, and dashed lines indicating unassigned residues. In the amino acid sequence of *Ma*MscL, the assigned and unassigned residues in the dipolar-coupling-based assignment are labeled in red and black, respectively.

assignments, in Table S1. As demonstrated in Figure 3A, a sequential walk along the backbone resonances was established through a combination of 3D correlation experiments, such as NCACX, NCOCX, and CONCA, resulting in unambiguous backbone and side-chain assignments for 73% of the residues (73 out of 101) of *Ma*MscL (Figure 3B), including all residues in the transmembrane domain. All of the resonance assignments have been deposited into the Biological Magnetic Resonance Data Bank (BMRB ID 52012).

Based on the assigned chemical shifts, the secondary structure of *Ma*MscL was predicted by a chemical shift index (CSI) and the TALOS+ program (Figure 3C). In our previous study, we determined the secondary structure of *Ma*MscL in synthetic lipid bilayers using solid-state NMR.[30] The overall secondary structure of *Ma*MscL in native cellular membranes closely resembles that observed in synthetic lipid bilayers, as demonstrated by solid-state NMR, and in detergent micelles, as revealed by X-ray crystallography (Figure S9). The insensitivity of the *Ma*MscL structure to the membrane environments can be attributed to its inherent rigidity, as demonstrated by the high-order parameters predicted by the TALOS+ program based on the assigned chemical shifts (Figure S10).[34] However, while most residues exhibit similar chemical shifts in both native and synthetic membranes (Figure S11), the signals from water-accessible residues S35/G62/V65/S67/G69 of *Ma*MscL in synthetic lipid bilayers are not observed in the water-edited spectrum of *Ma*MscL in native cellular membranes (Figure S12A).[35] As shown in Figure S12B,C, most residues exhibit similar sensitivities in the water-edited 2D NCA spectra of *Ma*MscL in native cellular

membranes and synthetic lipid bilayers, which excludes the possibility that other factors, such as the amount of labeled *Ma*MscL in each sample and the experimental parameters performed on each sample, are responsible for the disappearance of these signals. The difference in water accessibilities of these residues is likely due to different interactions in different membrane environments, such as interactions of *Ma*MscL with coexpressed molecular components in native cellular membranes.[16,17]

Potential For Collecting Distance Restraints for 3D Structure Determination Using Cellular Membrane Samples

Furthermore, both the complete suppression of background protein signals and sufficient spectral sensitivity of target protein signals are necessary requirements for collecting distance restraints using the 2D $^{13}C-^{13}C$ correlation spectra. In this study, we utilized the 2D $^{13}C-^{13}C$ spectrum of artificially prepared *Ma*MscL proteoliposomes as a reference. Notably, the 2D $^{13}C-^{13}C$ spectrum of *Ma*MscL in cellular membranes exhibits no background protein signals, except for signals from lipids (Figure 4A). The presence of lipid signals is expected, since lipids are also isotope-labeled during protein expression.

However, the signals of the lipids may potentially interfere with the assignment of distance restraints. To ensure an unambiguous assignment of the distance restraints, it is crucial to distinguish between protein and lipid signals. The assignment of lipid signals was confirmed by $^1H-^{13}C$ correlation spectra in both solid-state and solution NMR. In solid-state NMR, we recorded a $^1H-^{13}C$ INEPT (Insensitive
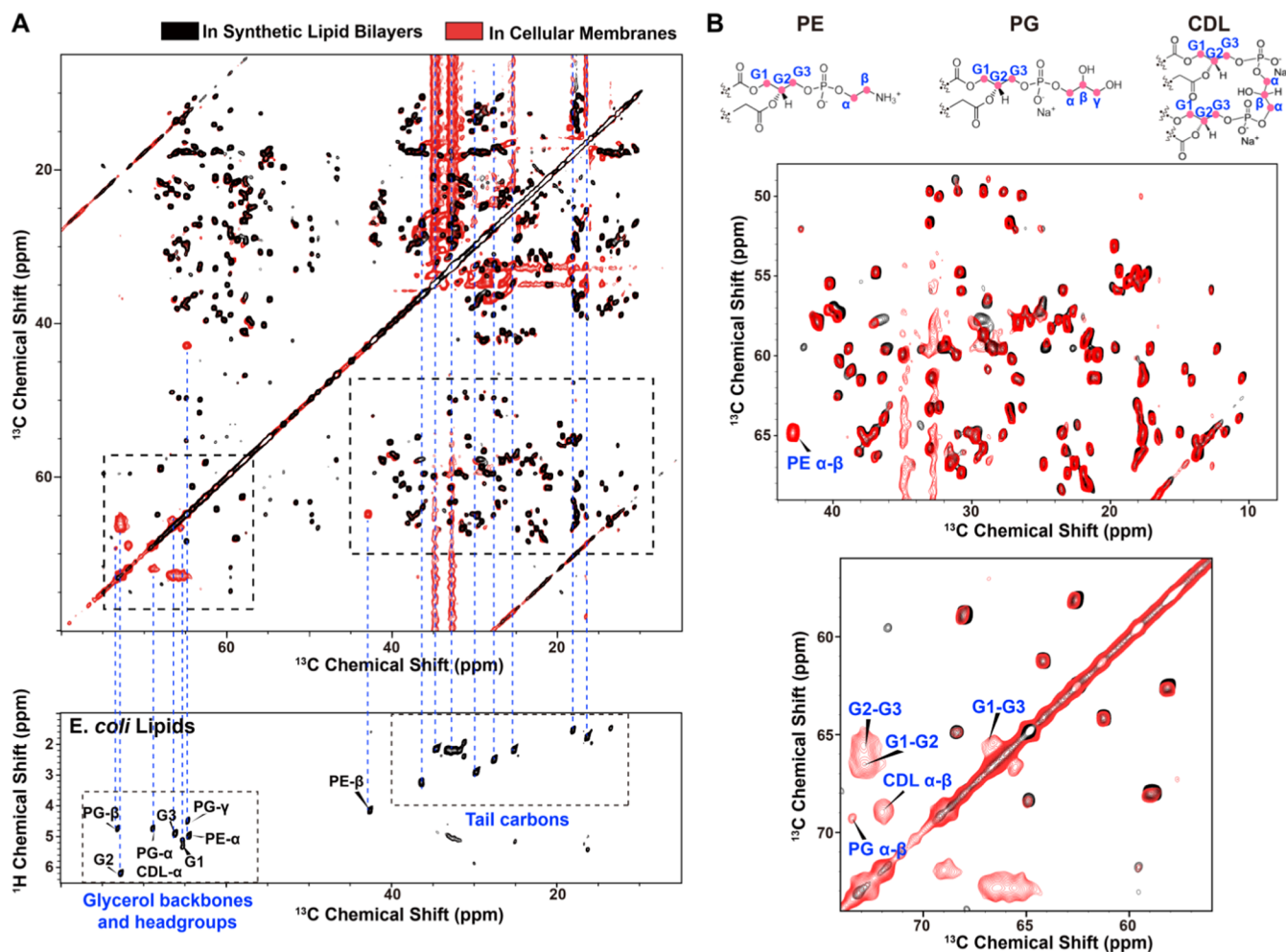
Figure 4. No signals from background proteins are present in the 2D $^{13}C-^{13}C$ spectrum of the MaMscL native cellular membrane sample. (A) Superimposition of 2D DARR spectra of MaMscL in native cellular membranes and synthetic lipid bilayers. All additional signals in the spectrum of the MaMscL cellular membrane sample are from lipids, which were assigned based on the $^1H-^{13}C$ INEPT spectrum of $E.$ $coli$ lipids. (B) Molecular structure formulas of phospholipids PE, PG, and CDL. Zoomed-in CA region of the superimposed 2D DARR spectra of MaMscL in native cellular membranes and synthetic lipid bilayers, highlighting the assigned signals of the phospholipid headgroups.

Nuclei Enhanced by Polarization Transfer) spectrum using commercial $E.$ $coli$ lipids, which consisted of approximately 57% PE, 15% PG, 10% cardiolipin (CDL), and 18% other minor species. By analyzing the $^1H-^{13}C$ HSQC solution NMR spectra of commercial POPG, POPE, and cardiolipin, we identified the ^{13}C signals corresponding to the headgroups and glycerol backbone of anionic lipids (PG), zwitterionic lipids (PE), and CDL (Figure S13). Based on the determined chemical shifts of lipid groups, we assigned the lipid signals in the 2D $^{13}C-^{13}C$ spectrum of the MaMscL cellular membrane sample (Figure 4B). All lipid signals can be excluded during the assignment of distance restraints, enabling us to achieve the structure determination of MPs in native cellular membranes.

High-Quality Solid-State NMR Spectra of the Other Membrane Proteins in Cellular Membranes

We also obtained solid-state NMR spectra of other membrane proteins in native cellular membranes, such as the sugar transporters VsSemiSWEET and BjSemiSWEET. As shown in Figure 5A, the NCA spectra of VsSemiSWEET and BjSemi-SWEET samples prepared using the C43(DE3) strain exhibited background protein signals, whereas these signals were absent in the spectra of samples prepared using the

BL21(DE3) strain. The high spectral sensitivity, combined with the complete suppression of background protein signals, will enable us to achieve complete resonance assignments and collect distance restraints for structural characterization (Figure S14).

Unexpectedly, additional signals were observed in the NCA spectrum of BjSemiSWEET in cellular membranes. These signals are unlikely to be the widely present background protein signals with relatively weak sensitivities. To identify the origin of these signals, we performed a de $novo$ assignment and demonstrated that these signals arise from residues in BjSemiSWEET rather than background proteins (Figure 5B). As shown in Figure 5C, we have assigned NMR signals for nearly complete residues (81 of 86) of BjSemiSWEET in cellular membranes (BMRB ID 52197). It is noteworthy that residues exhibiting significant chemical shift changes, such as S33/A34/R35/D36, are mainly located in the protein−lipid interface, which may be more susceptible to the influence of lipids. This finding indicates that the conformation of BjSemiSWEET in native cellular membranes differs from that in synthetic lipid bilayers, suggesting the influence of the native cellular membrane on the protein conformation.
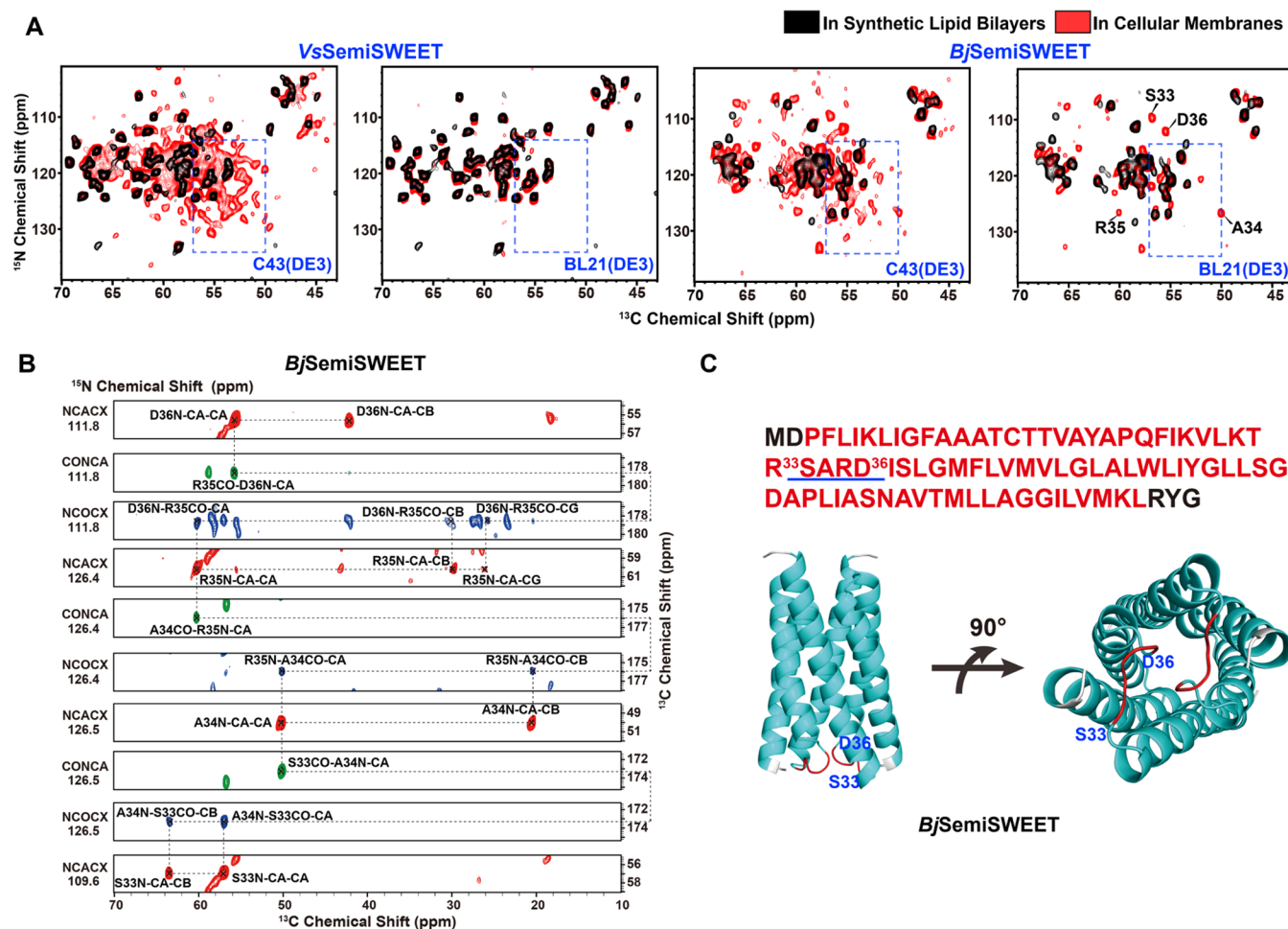
Figure 5. High-quality solid-state NMR spectra of the other membrane proteins in cellular membranes. (A) 2D NCA spectra of *Vs*SemiSWEET and *Bj*SemiSWEET in *E. coli* inner cellular membranes (red) prepared using C43(DE3) and BL21(DE3) expression strains. The NCA spectra of purified *Vs*SemiSWEET and *Bj*SemiSWEET reconstituted into *E. coli* lipid extracts (black) are superimposed onto the NCA spectra of native membranes as references. (B) Representative sequential assignments of S33−D36 of *Bj*SemiSWEET based on 3D NCACX, CONCA, and NCOCX spectra. (C) In the amino acid sequence of *Bj*SemiSWEET, assigned and unassigned residues are labeled in red and black, respectively. Mapping of the assignment of the residues into the structural model of *Bj*SemiSWEET predicted using AlphaFold;[36] assigned and unassigned residues are colored in cyan and gray, respectively. Residues S33−D36 in cellular membranes that exhibit significant chemical shift changes compared to those of the *Bj*SemiSWEET proteoliposome sample are labeled in red.

◼ DISCUSSION

MPs isolated from cellular membranes are likely to lose activity and native conformation required for functional analyses and structural studies.[37−39] Structural characterization of MPs in native cellular membranes provides valuable insights into their molecular mechanisms within the functional context. *In situ* studies offer several advantages over *in vitro* studies conducted in membrane mimic environments. *In vitro* studies typically involve the solubilization of membrane proteins from cellular membranes using detergents, which can potentially disrupt the native structures and functions of the MPs.[3] Furthermore, certain MPs lack available protocols for purification using detergents. These challenges introduced by the use of detergents in *in vitro* studies can be circumvented through *in situ* studies. However, *in situ* studies of MPs in native membranes face difficulties in achieving residue site-specific structural characterization due to poor spectral sensitivity and significant interference from background protein signals.

In this study, we address these challenges and propose a feasible approach for achieving complete resonance assignments of MPs in native cellular membranes. We employ a combination of various strategies in sample preparations, including optimized expression conditions, the use of "dual media", the BL21(DE3) strain, and the removal of nontarget membrane components. Importantly, our results demonstrate the suitability of *E. coli* BL21(DE3) as an expression strain for solid-state NMR cellular sample preparation. The use of the BL21(DE3) strain in the protocol effectively suppresses the labeling of background proteins without sacrificing the sensitivity of the target protein, in contrast to rifampicin treatment. While individual techniques can enhance the content of the target protein and reduce background proteins in native cellular membranes, only the combination of all four strategies can achieve complete suppression of background protein signals and maintain a sufficient concentration of the target protein. For example, previous studies on membrane proteins such as ASR, LR11, M2, Mistic, and the BAM complex have utilized the BL21(DE3) strain in cellular membrane sample preparations (Table S2). However, the quality of their solid-state NMR spectra did not meet the requirements for sensitivity and minimum interference in the resonance assignments.

Moreover, different proteins exhibit varying degrees of sensitivity to the membrane environment. For instance, the overall secondary structures of *Ma*MscL and *Vs*SemiSWEET in native cellular membranes are similar to those observed in synthetic lipid bilayers. In contrast, *Bj*SemiSWEET shows different conformations in native membranes compared with synthetic lipid bilayers. These results highlight the importance of native membrane environments in the structural characterization of membrane proteins. In cases where analyzing the structure of a membrane protein in its native membrane environment is not feasible, it becomes crucial to at least verify the nativeness of the structure in simplified membrane mimetics,[40] as the structures of certain membrane proteins, such as *Bj*SemiSWEET, are influenced by their membrane environments.

Our study represents a significant breakthrough in overcoming major challenges associated with achieving atomic-resolution structural characterization of membrane proteins in their native cellular membranes using solid-state NMR. This integrated approach holds great promise for revealing a wealth of knowledge about the biological function of membrane proteins in native cellular membranes. Furthermore, harnessing the power of cellular solid-state NMR in combination with complementary techniques such as in-cell NMR, EPR, fluorescence, and cellular cryo-ET can help reveal the intricate details of biomolecular functions within living cells as well as their significant roles in biological processes.

■ CONCLUSIONS

The secondary structure of *Ma*MscL in *E. coli* cellular membranes has been revealed using solid-state NMR spectroscopy. A novel protocol was employed to prepare cellular membrane samples, which combined various strategies to enhance the spectral sensitivity of the target protein and effectively suppress background protein signals. Notably, the BL21(DE3) strain exhibited exceptional capability in suppressing background protein labeling while maintaining the expression and labeling of the target protein. The resulting spectra of membrane proteins within cellular membranes exhibited sufficient sensitivity and minimal interference from background protein signals and further showed the potential for collecting distance restraints for 3D structure determination. The examination of different membrane proteins within cellular membrane environments highlights the importance of verifying the nativeness of membrane protein structures obtained from simplified membrane mimics. This study presents an opportunity for atomic-resolution structural analysis of membrane proteins within their native cellular membranes.

■ EXPERIMENTAL SECTION

Sample Preparation for Solid-State NMR Experiments

***Ma*MscL Proteoliposome Sample.** *Expression and Purification.* The pET-15b plasmid containing *Ma*MscL with a 6 × His tag was transformed at the N-terminus into *E. coli* C43(DE3) cells for expression. The *Ma*MscL colonies were inoculated into 100 mL of LB media containing 100 μg/mL ampicillin and allowed to grow overnight at 310 K. 20 mL of the cell suspension was transferred to 1 L of fresh LB media, and incubation was continued at 310 K until OD600 reached 0.7−0.8. The cells were harvested and then suspended in 250 mL of M9 media (4 g/L ^{13}C glucose, 1 g/L ^{15}N NH$_4$Cl), and incubation was continued at 310 K for 30 min until the OD reached 0.8−0.9. 1 mM IPTG (isopropyl-β-D-thiogalactoside)

was added to induce protein expression at 310 K for 5 h. The cells were harvested by centrifugation and suspended in 40 mL of lysis buffer (20 mM Tris, 100 mM NaCl, pH 8.0). To purify the target protein, the cells were lysed by ultrasonication. The lysate was centrifuged at 4629*g* for 10 min to remove unbroken cells and larger cell debris. The total cell membranes were collected by centrifugation at 58,545*g* for 1 h and then solubilized into 1% (w/v) sodium *N*-lauroylsarcosinate at 277 K overnight.

The *Ma*MscL was purified on a 2 mL Ni-IDA resin using 10 column volumes (CVs) of wash buffer [20 mM Tris, 100 mM NaCl, 20 mM imidazole, 0.3% (w/v) DM, pH 8.0], followed by 5 CVs of elution buffer (20 mM Tris, 100 mM NaCl, 300 mM imidazole, 0.3% DM, pH 8.0). The yield of pure *Ma*MscL was approximately 35 mg/L.

Reconstitution. To reconstitute the purified *Ma*MscL protein into *E. coli* liposomes, we prepared *E. coli* lipid stocks at a concentration of 5 mg/mL through hydration and ultrasonication. The lipids were then dissolved in 2% (w/v) *n*-octyl-β-glucoside (OG) and mixed with purified *Ma*MscL protein in a protein-to-lipid molar ratio of 1:26. After incubating the protein−lipid-detergent mixture at 291 K for 2 h, it was transferred into an 8 kDa dialysis bag and dialyzed against a dialysis buffer (20 mM Tris, pH 8.0) using an internal-to-external ratio of 1:500 (v/v). The dialysis buffer was changed every 24 h, and after 5 days of dialysis, *Ma*MscL protein−liposomes were collected through ultracentrifugation at 419,832*g* for 3 h. The liposomes were then freeze-dried and packed with 30% (w/w) H$_2$O into a 3.2 mm rotor (thin-wall) for solid-state NMR experiments.

***Vs*SemiSWEET Proteoliposome Sample.** *Expression and Purification.* *Vs*SemiSWEET was expressed in *E. coli* BL21(DE3) cells using a pET28a-*Vs*SemiSWEET plasmid with an N-terminal 6 × His tag. *Vs*SemiSWEET colonies were inoculated into 100 mL of LB media containing Kanamycin (100 μg/mL) and grown overnight at 310 K. Then, 20 mL of cell suspension was diluted into 1 L of fresh LB media and allowed to grow at 310 K. When the OD600 reached 0.8−0.9, cells were harvested by centrifugation and resuspended in 250 mL of M9 media (4 g/L ^{13}C glucose, 1 g/L ^{15}N NH$_4$Cl) and incubated at 310 K for 30 min. Next, 1 mM IPTG was added to induce protein expression at 310 K. Cells were collected by centrifugation after 5 h and resuspended in a lysis buffer (20 mM Tris, 100 mM NaCl, pH 8.0) followed by ultrasonication until clear. The lysate was then subjected to a low-speed centrifugation at 4629*g* for 10 min to remove unbroken cells and larger cell debris. The total cell membranes were collected by high-speed centrifugation at 58,545*g* for 1 h. The membranes were dissolved overnight in 1% (w/v) sodium *N*-lauroylsarcosinate at 277 K. The *Vs*SemiSWEET was then purified using 2 mL of Ni-IDA resin, with 10 CVs of wash buffer [20 mM Tris, 100 mM NaCl, 20 mM imidazole, 0.2% (w/v) DM, pH 8.0], followed by 5 CVs of elution buffer (20 mM Tris, 100 mM NaCl, 300 mM imidazole, 0.3% DM, pH 8.0). Approximately 30−35 mg of *Vs*SemiSWEET was purified from 1 L of M9 culture.

Reconstitution. The purified *Vs*SemiSWEET was reconstituted into *E. coli* liposomes by dialysis. The 5 mg/mL *E. coli* lipid stocks were prepared by hydration and ultrasonication. The lipids were dissolved in 2% (w/v) OG and mixed with purified *Vs*SemiSWEET at a protein-to-lipid ratio of 1:0.6 (w/w). The mixture was then incubated at 291 K for 2 h. Subsequently, the mixture was subjected to dialysis at 291 K for 6 days against an external solution of 20 mM Tris, pH 8.0. The *Vs*SemiSWEET protein−liposomes were collected by ultracentrifugation at 419,832*g* for 3 h and then freeze-dried. The dried complexes were rehydrated with 30% (w/w) water and packed into a 3.2 mm rotor (thin-wall) for solid-state NMR experiments.

***Bj*SemiSWEET Proteoliposome Sample.** *Expression and Purification.* *Bj*SemiSWEET were expressed in *E. coli* BL21(DE3) cells using a pET21a-*Bj*SemiSWEET plasmid with a C-terminal 6 × His tag. *Bj*SemiSWEET colonies were inoculated into 100 mL of LB media containing 100 μg/mL ampicillin and grown overnight at 310 K. Subsequently, 20 mL of cell suspension was diluted into fresh LB media (1 L) and cultured at 310 K until the cells reached an OD600 of 1.1−1.2, and at this point, they were harvested by centrifugation. The cells were suspended in 250 mL of M9 media (2 g/L ^{13}C glucose,

1 g/L ^{15}N NH$_4$Cl) and allowed to grow for 30 min at 310 K before being induced by adding 1 mM IPTG. After 5 h of target protein expression at 310 K, cells were collected by centrifugation, resuspended in lysis buffer (20 mM Tris, 100 mM NaCl, pH 8.0), and then lysed using ultrasonication. The lysate was then subjected to a low-speed centrifugation at 4629g for 10 min to remove unbroken cells and larger cell debris. The total cell membranes were collected by high-speed centrifugation at 58,545g for 1 h. The membranes were dissolved overnight in 1% (w/v) sodium N-lauroylsarcosinate at 277 K. BjSemiSWEET was then purified using 2 mL of Ni-IDA resin with 10 CVs of wash buffer [20 mM Tris, 100 mM NaCl, 20 mM imidazole, 0.2% (w/v) DPC, pH 8.0], followed by 5 CVs of elution buffer (20 mM Tris, 100 mM NaCl, 300 mM imidazole, 0.2% DPC, pH 8.0). Approximately 35−40 mg of BjSemiSWEET was purified from 1 L of M9 culture.

Reconstitution. To reconstitute the purified BjSemiSWEET into *E. coli* liposomes, *E. coli* lipid stocks were prepared at a concentration of 5 mg/mL through hydration and ultrasonication. The lipids were dissolved in 2% (w/v) OG and mixed with purified BjSemiSWEET at a protein-to-lipid ratio of 1:1.25 (w/w). The mixture was then incubated at 293 K for 2 h. Subsequently, the protein, detergent, and lipid mixture were dialyzed for 7 days at 285 K against a dialysis buffer containing 20 mM Tris, pH 7.7. On the sixth day, the dialysis buffer was changed to 10 mM Tris, and on the seventh day, to 5 mM Tris. The BjSemiSWEET protein−liposomes were collected by ultra-centrifugation at 419,832g for 3 h and then freeze-dried. The dried complexes were rehydrated with 30% (w/w) water and packed into a 3.2 mm rotor (thin-wall) for solid-state NMR experiments.

***Ma*MscL Cellular Membrane Sample.** *Expression of MaMscL.* The *Ma*MscL gene was expressed with an N-terminal 6xHis tag using the pET-15b plasmid in *E. coli* C43(DE3), BL21(DE3), or Rosetta cells. The *Ma*MscL colonies were inoculated into unlabeled LB media containing 100 μg/mL ampicillin at 310 K for 8 h. 1 mL of the culture was centrifuged and then resuspended in 100 mL of unlabeled media. It was incubated overnight at 310 K. All 100 mL of bacterial culture was inoculated into 900 mL of unlabeled media, and incubation was continued at 310 K until the OD600 reached approximately 0.8. The cells were harvested and then suspended in 250 mL of isotope-labeled M9 media (6 g/L ^{13}C glucose, 1 g/L ^{15}N NH$_4$Cl), and incubation was continued at 310 K for 10 min. 1 mM IPTG was added to induce protein expression for 5 h at 310 K (rifampicin treatment: after adding IPTG to induce protein expression for 10 min, rifampicin was added to a final concentration of 100 μg/mL). The cells were collected by centrifugation and resuspended in a lysis buffer (20 mM Tris, 100 mM NaCl, pH 8.0), and then, they were lysed by ultrasonication. The lysate was then subjected to a low-speed centrifugation at 4629g for 10 min to remove unbroken cells and larger cell debris. The total cell membranes were collected by high-speed centrifugation at 58,545g for 1 h.

Cellular Membrane Isolation. The cell membranes from 250 mL of isotope-labeled culture were resuspended in a lysis buffer (20 mM Tris, 100 mM NaCl, pH 8.0) and sonicated until the solution was clarified. Inner and outer membrane fractions were separated by using sucrose gradient centrifugation. Briefly, 2.7 mL of 60% (w/v) sucrose, 3.5 mL of 51% (w/v) sucrose, 3 mL of 35% (w/v) sucrose, and 4 mL of the sample were added successively into the buffer (20 mM Tris, 100 mM NaCl, pH 8.0) system. The gradients were centrifuged in an SW-40 Ti rotor (Beckman) at 169,818g for 16 h. The inner membranes were harvested at the interface between the 35 and 51% sucrose layers with a syringe, and the outer membranes were harvested at the interface between the 51 and 60% sucrose layers. 2 mL of the inner membrane sample was diluted with water to fill up an 8.9 mL Beckman centrifuge tube, and it was centrifuged at 419,832g for 3 h to collect the inner membranes. After freeze-drying, the inner membranes were rehydrated with 30% (w/w) water and packed into a 3.2 mm rotor (thin-wall) for solid-state NMR experiments.

***Vs*SemiSWEET Cellular Membrane Sample.** The method used for *Vs*SemiSWEET expression was similar to that described in the *Vs*SemiSWEET proteoliposome sample preparation. However, the OD600 value of the cells before switching from unlabeled to isotopically enriched media was adjusted from 0.8−0.9 to 1.3−1.4, and the incubation time prior to adding IPTG was shortened from 30 to 10 min. The procedures for cellular membrane isolation and inner membrane collection are the same as described above.

***Bj*SemiSWEET Cellular Membrane Sample.** The method used for *Bj*SemiSWEET expression was similar to that described in the *Bj*SemiSWEET proteoliposome sample preparation. However, the incubation time prior to adding IPTG was shortened from 30 to 10 min. The methods of cellular membrane isolation and inner membrane collection are the same as described above, with the exception that the pH of the buffer used for the sucrose gradient was adjusted from 8.0 to 8.2.

Quantitative Characterization of Protein Components in Cellular Membrane Sample

Quantitative Characterization of Labeled Proteins. The procedures for sample preparation were identical to those described in the *Ma*MscL cellular membrane sample preparation. The sample contains labeled *Ma*MscL, labeled background proteins, and other components. Both labeled *Ma*MscL and labeled background proteins in the inner membranes can be detected by a 1D ^{15}N NMR experiment. The amount of these labeled proteins was calculated by analyzing the ^{15}N signal intensity as a reference to that of *Ma*MscL in synthetic lipid bilayers, approximately.

Quantitative Characterization of Labeled *Ma*MscL. The procedures for sample preparation were identical to those described in the *Ma*MscL cellular membrane sample preparation. To distinguish signals from labeled background proteins and labeled *Ma*MscL, we performed a 2D NCA NMR experiment and compared the signal intensity of isolated cross-peaks in 2D NCA spectra from *Ma*MscL in inner membranes to that in synthetic lipid bilayers. The contents of labeled background proteins can be calculated by subtracting the labeled *Ma*MscL content from the labeled protein content.

Cell Growth Assays

Cells of BL21(DE3), Rosetta and C43(DE3) carrying the target genes (in the pET-15b vector) were cultured and induced, respectively. The procedures for protein expression were identical to those described in the *Ma*MscL cellular membrane sample preparation. The OD600 was measured every hour for up to 5 h after the adding of IPTG. The experimental traces are representative of three independent experiments. The error bars represent standard deviations.

Solid-State NMR Experiments

All solid-state NMR experiments for resonance assignment were conducted on a Bruker Avance 800 MHz (^{1}H Larmor frequency) spectrometer equipped with a 3.2 mm E-free triple-resonance HCN magic-angle spinning (MAS) probe. The experimental temperature was 273 K, and the MAS frequency was 10.5 kHz. In multidimensional dipolar-coupling-based experiments, polarization transfer between ^{15}N and ^{13}C was set up through SPECIFIC CP,[41] and ^{13}C−^{13}C correlations were performed using dipolar-assisted rotational resonance (DARR).[42] The typical 90° pulse lengths were 3.1 μs for ^{1}H, 4.1 μs for ^{13}C, and 6.7 μs for ^{15}N. The decoupling of 70 kHz was used during the acquisition and indirect chemical shift evolution. The ^{13}C chemical shifts were referenced to adamantine as external referencing standards (40.48 ppm for the adamantane ^{13}C downfield peak), and the ^{15}N chemical shifts were indirectly referenced to liquid NH$_3$ according to the gyromagnetic ratios. The experimental conditions for the water-edited NCA experiment were optimized for a 2.5 ms Gaussian pulse and a 1 ms ^{1}H T$_2$ filter to select the magnetization of water. The ^{1}H−^{1}H mixing time of 2.5 ms and ^{1}H−^{15}N cross-polarization contact time of 300 μs were applied to transfer ^{1}H polarization from water to the protein and prevent unwanted protein−protein ^{1}H spin diffusion. All of the solid-state NMR experimental data were processed by NMRPipe[43] software and analyzed using Sparky.

■ ASSOCIATED CONTENT

Supporting Information

The Supporting Information is available free of charge at https://pubs.acs.org/doi/10.1021/jacsau.3c00564.

Quantitative characterization and SDS-PAGE analysis of cellular membrane samples; 2D NCA spectra of *Ma*MscL cellular membrane samples in intermediate states of cell growth; effect of the rifampicin treatment; cell growth during protein expression using *E. coli* expression strains Rosetta and BL21(DE3); 2D planes extracted from the 3D spectra of *Ma*MscL in native cellular membranes; *Ma*MscL secondary structure in different environments; residue-specific order parameters of *Ma*MscL in native cellular membranes; site-specific chemical shift perturbations of *Ma*MscL in native cellular membranes and synthetic lipid bilayers; water accessibility in *Ma*MscL; assignments of commercial POPE, POPG, and CDL headgroups; 2D DARR spectra of *Bj*SemiSWEET in native cellular membranes; summary of the solid-state NMR experiments and sample information; and summary of conditions for preparing native cellular membrane samples in previous studies (PDF)

■ AUTHOR INFORMATION

Corresponding Authors

Huayong Xie − *National Center for Magnetic Resonance in Wuhan, State Key Laboratory of Magnetic Resonance and Atomic and Molecular Physics, Wuhan Institute of Physics and Mathematics, Wuhan National Laboratory for Optoelectronics, Innovation Academy for Precision Measurement Science and Technology, Chinese Academy of Sciences, Wuhan 430071, P. R. China;* ⓞ orcid.org/0000-0003-2865-6557; Email: xiehuayong@apm.ac.cn

Jun Yang − *Interdisciplinary Institute of NMR and Molecular Sciences, School of Chemistry and Chemical Engineering, The State Key Laboratory of Refractories and Metallurgy, Wuhan University of Science and Technology, Wuhan 430081, P. R. China; National Center for Magnetic Resonance in Wuhan, State Key Laboratory of Magnetic Resonance and Atomic and Molecular Physics, Wuhan Institute of Physics and Mathematics, Wuhan National Laboratory for Optoelectronics, Innovation Academy for Precision Measurement Science and Technology, Chinese Academy of Sciences, Wuhan 430071, P. R. China;* ⓞ orcid.org/0000-0002-4480-5340; Email: yangjun@wipm.ac.cn

Authors

Yan Zhang − *National Center for Magnetic Resonance in Wuhan, State Key Laboratory of Magnetic Resonance and Atomic and Molecular Physics, Wuhan Institute of Physics and Mathematics, Wuhan National Laboratory for Optoelectronics, Innovation Academy for Precision Measurement Science and Technology, Chinese Academy of Sciences, Wuhan 430071, P. R. China; University of Chinese Academy of Sciences, Beijing 100049, P. R. China*

Yuefang Gan − *National Center for Magnetic Resonance in Wuhan, State Key Laboratory of Magnetic Resonance and Atomic and Molecular Physics, Wuhan Institute of Physics and Mathematics, Wuhan National Laboratory for Optoelectronics, Innovation Academy for Precision*

Measurement Science and Technology, Chinese Academy of Sciences, Wuhan 430071, P. R. China; University of Chinese Academy of Sciences, Beijing 100049, P. R. China

Weijing Zhao − *National Center for Magnetic Resonance in Wuhan, State Key Laboratory of Magnetic Resonance and Atomic and Molecular Physics, Wuhan Institute of Physics and Mathematics, Wuhan National Laboratory for Optoelectronics, Innovation Academy for Precision Measurement Science and Technology, Chinese Academy of Sciences, Wuhan 430071, P. R. China*

Xuning Zhang − *National Center for Magnetic Resonance in Wuhan, State Key Laboratory of Magnetic Resonance and Atomic and Molecular Physics, Wuhan Institute of Physics and Mathematics, Wuhan National Laboratory for Optoelectronics, Innovation Academy for Precision Measurement Science and Technology, Chinese Academy of Sciences, Wuhan 430071, P. R. China*

Yongxiang Zhao − *National Center for Magnetic Resonance in Wuhan, State Key Laboratory of Magnetic Resonance and Atomic and Molecular Physics, Wuhan Institute of Physics and Mathematics, Wuhan National Laboratory for Optoelectronics, Innovation Academy for Precision Measurement Science and Technology, Chinese Academy of Sciences, Wuhan 430071, P. R. China*

Complete contact information is available at:
https://pubs.acs.org/10.1021/jacsau.3c00564

Author Contributions

||Y.Z., Y.G., and W.Z. contributed equally to this work. **Zhang Yan** data curation, formal analysis, investigation, writing-original draft; **Yuefang gan** data curation, investigation, writing-original draft; **Weijing Zhao** data curation, investigation, writing-original draft; **Xuning Zhang** data curation, investigation; **Yongxiang Zhao** data curation, investigation; **Huayong Xie** investigation, supervision, writing-review & editing; **Jun Yang** conceptualization, funding acquisition, project administration, writing-review & editing.

Notes

The authors declare no competing financial interest.

■ ACKNOWLEDGMENTS

■ REFERENCES

(1) Ernst, M.; Robertson, J. L. The Role of the Membrane in Transporter Folding and Activity. *J. Mol. Biol.* **2021**, *433*, No. 167103.

(2) Thoma, J.; Burmann, B. M. Fake It 'Till You Make It-The Pursuit of Suitable Membrane Mimetics for Membrane Protein Biophysics. *Int. J. Mol. Sci.* **2021**, *22*, 50.

(3) Cross, T. A.; Sharma, M.; Yi, M.; Zhou, H. X. Influence of solubilizing environments on membrane protein structures. *Trends Biochem. Sci.* **2011**, *36*, 117−125.

(4) Baldus, M. A Solid View of Membrane Proteins In Situ. *Biophys. J.* **2015**, *108*, 1585−1586.

(5) Narasimhan, S.; Pinto, C.; Paioni, A. L.; van der Zwan, J.; Folkers, G. E.; Baldus, M. Characterizing proteins in a native bacterial environment using solid-state NMR spectroscopy. *Nat. Protoc.* **2021**, *16*, 893−918.

(6) Brown, L. S.; Ladizhansky, V. Membrane proteins in their native habitat as seen by solid-state NMR spectroscopy. *Protein Sci.* **2015**, *24*, 1333−1346.

(7) Medeiros-Silva, J.; Jekhmane, S.; Paioni, A. L.; Gawarecka, K.; Baldus, M.; Swiezewska, E.; Breukink, E.; Weingarth, M. High-resolution NMR studies of antibiotics in cellular membranes. *Nat. Commun.* **2018**, *9*, No. 3963.

(8) Theillet, F. X. In-Cell Structural Biology by NMR: The Benefits of the Atomic Scale. *Chem. Rev.* **2022**, *122*, 9497−9570.

(9) Theillet, F. X.; Binolfi, A.; Bekei, B.; Martorana, A.; Rose, H. M.; Stuiver, M.; Verzini, S.; Lorenz, D.; van Rossum, M.; Goldfarb, D.; et al. Structural disorder of monomeric alpha-synuclein persists in mammalian cells. *Nature* **2016**, *530*, 45−50.

(10) König, I.; Zarrine-Afsar, A.; Aznauryan, M.; Soranno, A.; Wunderlich, B.; Dingfelder, F.; Stuber, J. C.; Pluckthun, A.; Nettels, D.; Schuler, B. Single-molecule spectroscopy of protein conformational dynamics in live eukaryotic cells. *Nat. Methods* **2015**, *12*, 773−779.

(11) Baker, L. A.; Grange, M.; Grunewald, K. Electron cryo-tomography captures macromolecular complexes in native environments. *Curr. Opin. Struct. Biol.* **2017**, *46*, 149−156.

(12) Suzuki, M.; Mao, L.; Inouye, M. Single protein production (SPP) system in *Escherichia coli*. *Nat. Protoc.* **2007**, *2*, 1802−1810.

(13) Mao, L. L.; Inoue, K.; Tao, Y. S.; Montelione, G. T.; McDermott, A. E.; Inouye, M. Suppression of phospholipid biosynthesis by cerulenin in the condensed Single-Protein-Production (cSPP) system. *J. Biomol. NMR* **2011**, *49*, 131−137.

(14) Ding, X. Y.; Fu, R. Q.; Tian, F. De novo resonance assignment of the transmembrane domain of LR11/SorLA in *E. coli* membranes. *J. Magn. Reson.* **2020**, *310*, No. 106639.

(15) Baker, L. A.; Daniels, M.; van der Cruijsen, E. A. W.; Folkers, G. E.; Baldus, M. Efficient cellular solid-state NMR of membrane proteins by targeted protein labeling. *J. Biomol. NMR* **2015**, *62*, 199−208.

(16) Renault, M.; Tommassen-van Boxtel, R.; Bos, M. P.; Post, J. A.; Tommassen, J.; Baldus, M. Cellular solid-state nuclear magnetic resonance spectroscopy. *Proc. Natl. Acad. Sci. U.S.A.* **2012**, *109*, 4863−4868.

(17) Ward, M. E.; Wang, S. L.; Munro, R.; Ritz, E.; Hung, I.; Gor'kov, P. L.; Jiang, Y. J.; Liang, H. J.; Brown, L. S.; Ladizhansky, V. In Situ Structural Studies of Anabaena Sensory Rhodopsin in the *E. coli* Membrane. *Biophys. J.* **2015**, *108*, 1683−1696.

(18) Renault, M.; Pawsey, S.; Bos, M. P.; Koers, E. J.; Nand, D.; Tommassen-van Boxtel, R.; Rosay, M.; Tommassen, J.; Maas, W. E.; Baldus, M. Solid-State NMR Spectroscopy on Cellular Preparations Enhanced by Dynamic Nuclear Polarization. *Angew. Chem., Int. Ed.* **2012**, *51*, 2998−3001.

(19) Kaplan, M.; Cukkemane, A.; van Zundert, G. C. P.; Narasimhan, S.; Daniels, M.; Mance, D.; Waksman, G.; Bonvin, A.; Fronzes, R.; Folkers, G. E.; Baldus, M. Probing a cell-embedded megadalton protein complex by DNP-supported solid-state NMR. *Nat. Methods* **2015**, *12*, 649−652.

(20) Narasimhan, S.; Scherpe, S.; Paioni, A. L.; van der Zwan, J.; Folkers, G. E.; Ovaa, H.; Baldus, M. DNP-Supported Solid-State NMR Spectroscopy of Proteins Inside Mammalian Cells. *Angew. Chem., Int. Ed.* **2019**, *58*, 12969−12973.

(21) Medeiros-Silva, J.; Mance, D.; Daniels, M.; Jekhmane, S.; Houben, K.; Baldus, M.; Weingarth, M. H1-Detected Solid-State NMR Studies of Water-Inaccessible Proteins InVitro and InSitu. *Angew. Chem., Int. Ed.* **2016**, *55*, 13606−13610.

(22) Baker, L. A.; Sinnige, T.; Schellenberger, P.; de Keyzer, J.; Siebert, C. A.; Driessen, A. J. M.; Baldus, M.; Grunewald, K. Combined H-1-Detected Solid-State NMR Spectroscopy and Electron Cryotomography to Study Membrane Proteins across Resolutions in Native Environments. *Structure* **2018**, *26*, 161−170.

(23) Fu, R. Q.; Wang, X. S.; Li, C. G.; Santiago-Miranda, A. N.; Pielak, G. J.; Tian, F. In Situ Structural Characterization of a Recombinant Protein in Native *Escherichia coli* Membranes with Solid-State Magic-Angle-Spinning NMR. *J. Am. Chem. Soc.* **2011**, *133*, 12370−12373.

(24) Miao, Y. M.; Qin, H. J.; Fu, R. Q.; Sharma, M.; Can, T. V.; Hung, I.; Luca, S.; Gor'kov, P. L.; Brey, W. W.; Cross, T. A. M2 Proton Channel Structural Validation from Full-Length Protein Samples in Synthetic Bilayers and *E. coli* Membranes. *Angew. Chem., Int. Ed.* **2012**, *51*, 8383−8386.

(25) Jacso, T.; Franks, W. T.; Rose, H.; Fink, U.; Broecker, J.; Keller, S.; Oschkinat, H.; Reif, B. Characterization of Membrane Proteins in Isolated Native Cellular Membranes by Dynamic Nuclear Polarization Solid-State NMR Spectroscopy without Purification and Reconstitution. *Angew. Chem., Int. Ed.* **2012**, *51*, 432−435.

(26) Pinto, C.; Mance, D.; Julien, M.; Daniels, M.; Weingarth, M.; Baldus, M. Studying assembly of the BAM complex in native membranes by cellular solid-state NMR spectroscopy. *J. Struct. Biol.* **2019**, *206*, 1−11.

(27) Shahid, S. A.; Nagaraj, M.; Chauhan, N.; Franks, T. W.; Bardiaux, B.; Habeck, M.; Orwick-Rydmark, M.; Linke, D.; van Rossum, B. J. Solid-state NMR Study of the YadA Membrane-Anchor Domain in the Bacterial Outer Membrane. *Angew. Chem., Int. Ed.* **2015**, *54*, 12602−12606.

(28) Bersch, B.; Dorr, J. M.; Hessel, A.; Killian, J. A.; Schanda, P. Proton-Detected Solid-State NMR Spectroscopy of a Zinc Diffusion Facilitator Protein in Native Nanodiscs. *Angew. Chem., Int. Ed.* **2017**, *56*, 2508−2512.

(29) Li, J.; Guo, J. L.; Ou, X. M.; Zhang, M. F.; Li, Y. Z.; Liu, Z. F. Mechanical coupling of the multiple structural elements of the large-conductance mechanosensitive channel during expansion. *Proc. Natl. Acad. Sci. U.S.A.* **2015**, *112*, 10726−10731.

(30) Zhang, X. N.; Zhang, Y.; Tang, S. Y.; Ma, S. J.; Shen, Y.; Chen, Y. K.; Tong, Q.; Li, Y. Z.; Yang, J. Hydrophobic Gate of Mechanosensitive Channel of Large Conductance in Lipid Bilayers Revealed by Solid-State NMR Spectroscopy. *J. Phys. Chem. B* **2021**, *125*, 2477−2490.

(31) Kwon, S. K.; Kim, S. K.; Lee, D. H.; Kim, J. F. Comparative genomics and experimental evolution of *Escherichia coli* BL21(DE3) strains reveal the landscape of toxicity escape from membrane protein overproduction. *Sci. Rep.* **2015**, *5*, No. 16076.

(32) Xu, Y.; Tao, Y. Y.; Cheung, L. S.; Fan, C.; Chen, L. Q.; Xu, S.; Perry, K.; Frommer, W. B.; Feng, L. Structures of bacterial homologues of SWEET transporters in two distinct conformations. *Nature* **2014**, *515*, 448−452.

(33) Xuan, Y. H.; Hu, Y. B.; Chen, L. Q.; Sosso, D.; Ducat, D. C.; Hou, B. H.; Frommer, W. B. Functional role of oligomerization for bacterial and plant SWEET sugar transporter family. *Proc. Natl. Acad. Sci. U.S.A.* **2013**, *110*, E3685−E3694.

(34) Shen, Y.; Delaglio, F.; Cornilescu, G.; Bax, A. TALOS plus: a hybrid method for predicting protein backbone torsion angles from NMR chemical shifts. *J. Biomol. NMR* **2009**, *44*, 213−223.

(35) Luo, W. B.; Hong, M. Conformational Changes of an Ion Channel Detected Through Water-Protein Interactions Using Solid-State NMR Spectroscopy. *J. Am. Chem. Soc.* **2010**, *132*, 2378−2384.

(36) Jumper, J.; Evans, R.; Pritzel, A.; Green, T.; Figurnov, M.; Ronneberger, O.; Tunyasuvunakool, K.; Bates, R.; Zídek, A.; Potapenko, A.; et al. Highly accurate protein structure prediction with AlphaFold. *Nature* **2021**, *596*, 583−589.

(37) Martens, C.; Stein, R. A.; Masureel, M.; Roth, A.; Mishra, S.; Dawaliby, R.; Konijnenberg, A.; Sobott, F.; Govaerts, C.; McHaourab, H. S. Lipids modulate the conformational dynamics of a secondary multidrug transporter. *Nat. Struct. Mol. Biol.* **2016**, *23*, 744−751.

(38) Engberg, O.; Ulbricht, D.; Dobel, V.; Siebert, V.; Frie, C.; Penk, A.; Lemberg, M. K.; Huster, D. Rhomboid-catalyzed intramembrane proteolysis requires hydrophobic matching with the surrounding lipid bilayer. *Sci. Adv.* **2022**, *8*, No. eabq8303.

(39) Martens, C.; Shekhar, M.; Borysik, A. J.; Lau, A. M.; Reading, E.; Tajkhorshid, E.; Booth, P. J.; Politis, A. Direct protein-lipid interactions shape the conformational landscape of secondary transporters. *Nat. Commun.* **2018**, *9*, No. 4151.

(40) Zhou, H. X.; Cross, T. A. Influences of Membrane Mimetic Environments on Membrane Protein Structures. *Annu. Rev. Biophys.* **2013**, *42*, 361−392.

(41) Baldus, M.; Petkova, A. T.; Herzfeld, J.; Griffin, R. G. Cross polarization in the tilted frame: assignment and spectral simplification in heteronuclear spin systems. *Mol. Phys.* **1998**, *95*, 1197−1207.

(42) Takegoshi, K.; Nakamura, S.; Terao, T. 13C-H1 dipolar-assisted rotational resonance in magic-angle spinning NMR. *Chem. Phys. Lett.* **2001**, *344*, 631−637.

(43) Delaglio, F.; Grzesiek, S.; Vuister, G. W.; Zhu, G.; Pfeifer, J.; Bax, A. NMRPipe: A multidimensional spectral processing system based on UNIX pipes. *J. Biomol. NMR* **1995**, *6*, 277−293.